

# Holocene Moisture Variation Recorded by Aeolian Sand-Palaeosol Sequences of the Gonghe Basin, Northeastern Qinghai-Tibetan Plateau, China



LIU Bing<sup>1,2</sup>, ZHAO Hui<sup>1,\*</sup>, JIN Heling<sup>1</sup> and CHEN Fahu<sup>2,3</sup>

<sup>1</sup>Key Laboratory of Desert and Desertification, Northwest Institute of Eco-Environment and Resources, Chinese Academy of Science, Lanzhou 730000, China

<sup>2</sup>Key Laboratory of Western China's Environmental Systems, Ministry of Education, Lanzhou 73000, China

<sup>3</sup>Key Laboratory of Alpine Ecology, Institute of Tibetan Plateau Research, Chinese Academy of Sciences, Beijing 100101, China

**Abstract:** The northeastern Qinghai-Tibetan Plateau (QTP) of China is located at the triple junction of the Asian winter and summer monsoons and the westerlies, where paleoclimatic evolution has an important scientific significance for recognizing the spatial-temporal pattern of Asian monsoons in the past and predicting environmental change in the future. Nevertheless, the framework of the Holocene moisture variation and related mechanisms remain controversial, owing to complex hydroclimatic conditions triggered by the landform of the large mountain-arid basin. Here, we employed geochemical proxies from typical aeolian sand-palaeosol sequences in the Gonghe Basin, northeastern QTP, together with Optically Stimulated Luminescence (OSL) dating, to reconstruct the pattern of effective moisture variation and associated mechanisms in this region. Our results indicate that the regional effective moisture was at its lowest until 9–8 ka, and approached a maximum during 8–4/3 ka of the middle Holocene. Afterwards, the climate became relatively dry in general, but with a transient humid interval around 2–1 ka. Our geochemical evidence indicates that the dry early Holocene probably can be attributed to a strong winter monsoon forced by remnant ice sheet, combined with the high evaporation caused by solar insolation. Also, shifts of humid-dry are closely linked to the Asian summer monsoonal strength and therefore the balance of evaporation-precipitation in the middle and late Holocene. Thus, the pattern of the Holocene effective moisture variation is characterized as the ‘monsoon model’ in a closed intermontane arid and semi-arid basin near the western Asian monsoonal limit.

**Key words:** effective moisture, geochemical analysis, aeolian deposits, Holocene, Gonghe Basin

Citation: Liu et al., 2020. Holocene Moisture Variation Recorded by Aeolian Sand-Palaeosol Sequences of the Gonghe Basin, Northeastern Qinghai-Tibetan Plateau, China. *Acta Geologica Sinica (English Edition)*, 94(3): 668–681. DOI: 10.1111/1755-6724.14541

## 1 Introduction

Environmental changes of desert/dune fields in arid and semi-arid regions of the middle latitudes of the northern hemisphere are of particular importance throughout geological time. These changes have scientific significance for understanding modern surface processes and future environmental change trends in these key regions (Lu et al., 2005, 2013a; Sun et al., 2006; Mason et al., 2009; Yang et al., 2011, 2013, 2019; Fan et al., 2013, 2016; Jiang et al., 2018; Yang and Zhu, 2018). The desert/dune fields across the Asian summer monsoonal boundary zone of northern China (Fig. 1a) are not only a vital landscape and a source of atmospheric dust emission (Zhang et al., 2003; Xu et al., 2017, 2018), but are also typically ecologically fragile areas in relation to global climate change (Lu et al., 2013b; Li et al., 2014). In particular, regional climate/moisture is closely linked to the strength of summer monsoonal precipitation (Wang et al., 2005; Chen et al., 2015, 2016ab; Zhang et al., 2019),

which also generates crucial feedback for marine biochemical processes and global climate ecosystems (De Baar et al., 1995; Uno et al., 2009).

The northeastern QTP, composed mainly of several high-altitude mountains greater than 4000 m in height and the semi-arid and arid intermontane basins, i.e., the Qinghai Lake, Gonghe and Qaidam basins, is the most important component of the fragile landscape belt and farming-pastoral zone in northwestern China (Wang et al., 2011). Also, this region is situated at the triple junction of the Asian summer and winter monsoons, and the westerlies. Thus, this region is a focal point for tracing environmental evolution and feedback owing to its fragile natural ecology and hydrothermal sensitivity (Bryson, 1986). Since the late Quaternary, massive lake and aeolian deposits have developed in this region, which provides important archives for understanding past hydroclimatic changes (Shen et al., 2005; Liu et al., 2007, 2008; Lu et al., 2011, 2015; An et al., 2012; Cheng et al., 2013; Qiang et al., 2013ab; Yu and Lai, 2014; Zhang et al., 2016; Stauch et al., 2018). However, the pattern of the Holocene

\* Corresponding author. E-mail: hzhao@lzb.ac.cn

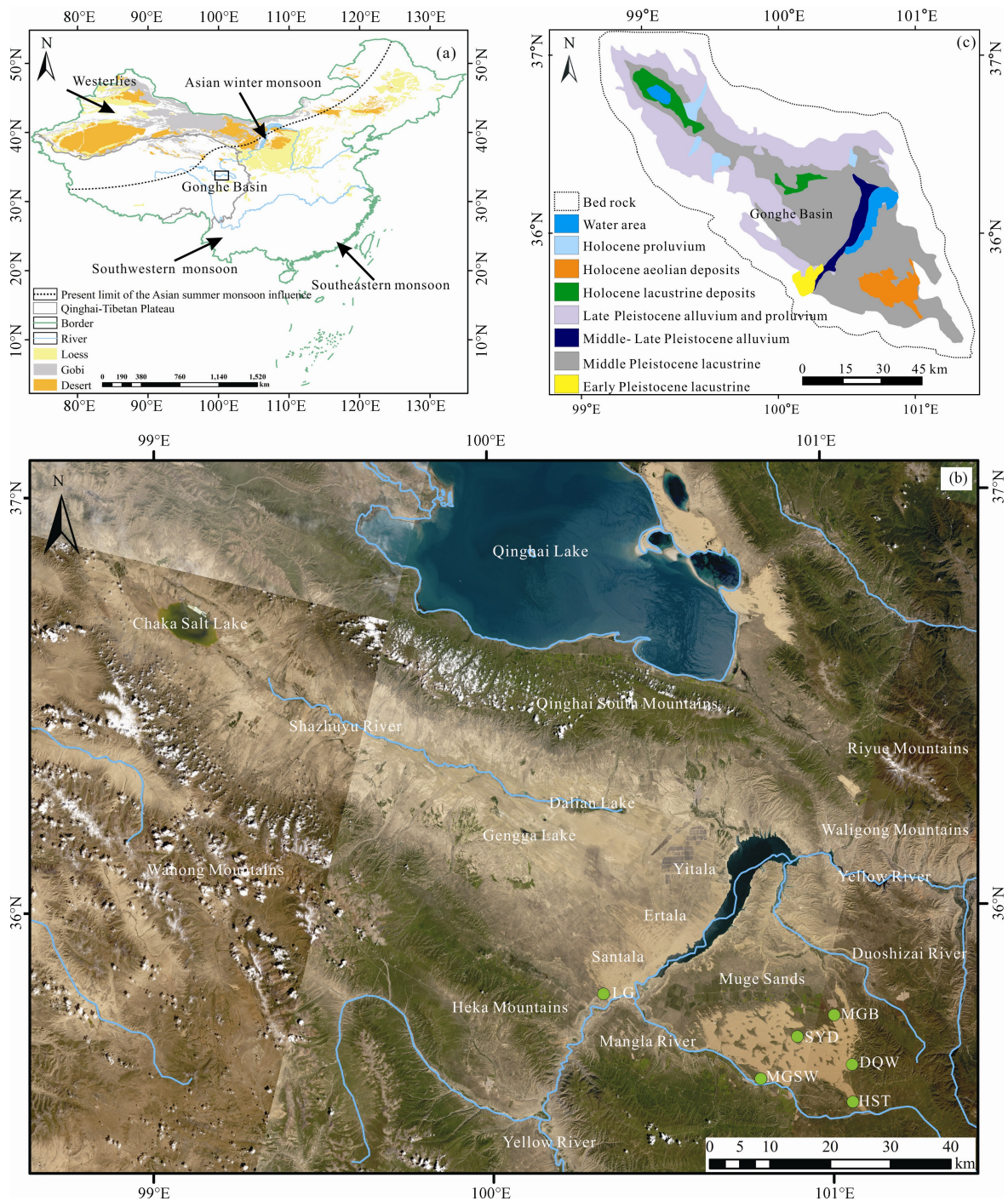


Fig. 1. Gonghe Basin location and representative aeolian sand-palaeosol/weak palaeosol sections.

(a) Map of the Gonghe Basin location (rectangle), black dashed line shows the Modern Asian summer monsoon boundary (Gao et al., 1962); (b) Representative aeolian sand-palaeosol / weak palaeosol sequences (green dots) in this study; (c) Stratigraphic distribution of the Gonghe Basin, modified from Sun et al., (2007). China basemap after China National Bureau of Surveying and Mapping Geographical Information.

climatic/effective moisture variation still remains controversial because of the complex hydroclimatic conditions triggered by the landform of the large mountain-arid basin. For example, aeolian deposits (Yu and Lai, 2014) and different proxies from numerous lakes (Shen et al., 2005; Liu et al., 2007, 2008, 2014a; An et al., 2012; Liu et al., 2012; Qiang et al., 2013a; Herzsuh et al., 2014; Jin et al., 2016) suggest a strong Asian summer

monsoon and moisture occurred during the early and middle Holocene. Also, numerous studies suggest that a wet climate dominated the region in the middle Holocene to even early-late Holocene from sand and loess archives, as well as lake sediments (Xu et al., 1982; Dong et al., 1993; Gao et al., 1993; Lu et al., 2011, 2015; Cheng et al., 2013; Qiang et al., 2013b, 2016; Liu et al., 2014b; Chen et al., 2016a; Ding et al., 2019). In fact, the discrepancies

between these results are probably due to the interpretations of multiple proxies and dating reliability of different sediments, while also being closely linked to the complex hydroclimatic conditions forced by the large mountain-arid basin landform. Therefore, proxies with significant and reliably dated sediments that were less influenced by local conditions have a unique potential for assessing previous conflicting results.

In this study, we used geochemical approaches from four well-dated sections around the middle and eastern Gonghe Basin, combined with OSL dating of fine- and coarse-grain quartz and feldspar, to reconstruct and synthesize moisture variability during the Holocene. The main objectives are: (1) to recover the Holocene moisture change history based on different indicators of geochemical parameters and to verify their commonality and differences; (2) to probe the potential forcing mechanisms of the evolution of the regional environment.

## 2 Regional Settings

The Gonghe Basin is a closed intermontane arid and semi-arid basin in the northeastern margin of the QTP, China, which extends from 98°46'E to 101°22'E and from 35°27'N to 36°56'N, with an area of 13,800 km<sup>2</sup> (Dong et al., 1993). The basin is bounded by Xiqing Mountain of the Qinling Mountain system to the east, Heka, Ela and Wahong mountains of the Kunlun system to the south and southeast, Qinghai South Mountain to the north, and Waligong, Laji and Riyue mountains to the northeast (Fig. 1b). This basin started to form at the end of the Paleogene and subsided until the early- to mid-Pleistocene (Xu et al., 1984). Since the late Pleistocene, the regional ground surface has been dominated by aeolian deposits in a relatively cold-dry and windy climatic context (Fig. 1c). At present, the region has predominantly fixed, semi-fixed and semi-mobile sand dunes which are distributed on

Muge Sands, Talatan (Yitala, Ertala, and Santala), and the middle and lower reaches of the Shazhuyu River. The region has a cold and dry alpine and arid/semi-arid climate, with an annual temperature and precipitation of 1.0–5.2°C and 311.1–402.1 mm, respectively, with more than 80% of the rainfall occurring in summer owing to the influence of the Asian summer monsoon. In contrast, annual evaporation is 1528–1937 mm. The natural vegetation is represented by obvious vertical zonation from low to high elevation of the basin. Specifically, the vegetation is mainly characterized by desert and desert steppe below 3000 m, except for some mosaic meadows in lowland areas fed by ground water. Around 3200 m, the vegetation consists of typical steppe near the diluvial fan of the piedmont. Over 3600 m, subalpine meadows dominate the community along the mountainside in the eastern Gonghe Basin (Qiang et al., 2016).

## 3 Samples and Methods

### 3.1 Samples

Aeolian deposits are widely distributed throughout the eastern and middle part of the Gonghe Basin, northeastern QTP, i.e., the Muge Sands, Yitala, Ertala and Santala. In this study, four representative aeolian sand-palaeosol/weak palaeosol sequences were investigated around Muge Sands and Santala in the middle of the Gonghe Basin. The location of the sections and detailed lithological characteristics are as follows (Figs. 1 and 2):

The HST section lies on the margin of the southeastern Muge Sands (35.53°N, 101.06°E), at an altitude of 3352 m. The section consists mainly of aeolian sand and palaeosol/weak palaeosol. The upper 140 cm is grayish weak palaeosol, with a dense plant root system. From 140 cm to 170 cm, it is comprised of relatively loose aeolian sand. A typical sandy palaeosol is developed from 170–215 cm, grayish to black colored, containing numerous

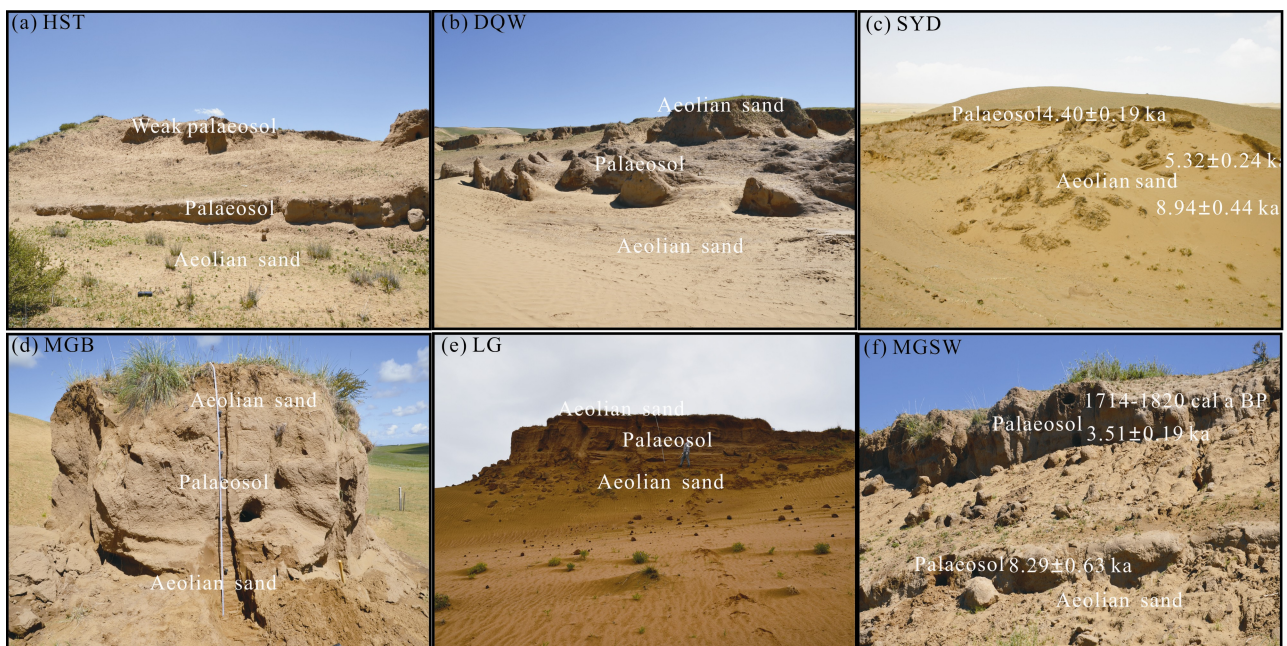


Fig. 2. Lithostratigraphic units of the studied sections in the Gonghe Basin.

white spots and mycelia. The yellow aeolian sand accumulated in the bottom of the section lies beneath 215 cm, with a visible thickness of 40 cm.

The DQW section lies on the eastern edge of the Muge Sands (35.62°N, 101.06°E) at an elevation of 3496 m. The stratum is grayish-orange, loose aeolian sand in 0–180 cm, except for the sod horizon at about the top 10 cm of the section. From 180 cm to 380 cm, the deposits are dominated by black brown sandy palaeosol, poorly to moderately sorted, with increasing white spots and mycelia. Below 380 cm, there is an accumulation of orange-grayish fine sand, relatively well-sorted and clearly unconsolidated.

The MGB section lies on the northeastern edge of the Muge Sands (35.74°N, 101.01°E, and 3405 m above sea level), and is composed of five aeolian sand and four palaeosol/weak palaeosols, with a total thickness of 550 cm. The aeolian sand is pale-orange silty fine sand, moderately sorted, slightly compacted. The palaeosol/weak palaeosol is grayish-taupe very fine sand and fine sand, compacted, moderately sorted, containing plentiful white mycelia and wormholes.

The LG section lies in southern Santala (35.80°N, 100.33°E, and 3279 m above sea level), in the middle of the Gonghe Basin, with a thickness of 525 cm, and consists of one sod horizon, six aeolian sand and five palaeosol/weak palaeosols. The sod horizon consists of orange fine sand, loose to slightly compacted, moderately sorted, with an abundance of modern plant roots; the aeolian sand is grayish-yellow to claybank fine and medium sand, loose to slightly hard, relatively well-sorted; the palaeosol/weak palaeosols are pale with black/gray silty fine sand, slightly hard to very hard, poorly sorted, containing massive white mycelia.

### 3.2 Method

Samples were collected from the aforementioned sections at 5 cm intervals from the palaeosol/weak palaeosol layers and 5–10 cm intervals from the aeolian sand layers for analysis of the geochemical elements and total organic carbon (TOC) content. The geochemical work was performed at the Key Laboratory of Desert and Desertification, Cold and Arid Regions Environmental and Engineering Research Institute, Chinese Academy of Sciences. Elemental content was determined by a wavelength dispersion-type X-ray fluorescence spectrometer (type: Axios), and the procedures followed were as follows. First, the samples were dried and ground, then sifted through a 200-mesh screen. Then 4-g powdered samples were placed into a mold with boric acid for the edge and base, to be pressed into round discs (32-mm diameter) at 30-ton pressure and 105°C. The discs were measured with a spectrometer (type: Axios), using a super-long, sharp-pointed ceramic X-ray light tube (4-kW power) and a pipe flow of 160 mA. The estimated error was less than 5%. In this paper, elemental results consisted of major elements, i.e., Al<sub>2</sub>O<sub>3</sub>, Fe<sub>2</sub>O<sub>3</sub>, CaO, MgO, Na<sub>2</sub>O, K<sub>2</sub>O and trace elements, i.e., Rb, Sr, Mn, Cr, Co, Ni, Ba, for calculating the geochemical parameters. The geochemical parameters were mainly comprised of the eluviation coefficient [(Al<sub>2</sub>O<sub>3</sub>+Fe<sub>2</sub>O<sub>3</sub>)/(CaO+MgO+Na<sub>2</sub>O+

K<sub>2</sub>O)], Rb/Sr ratio, moisture index [(Al+Fe+Mn)/(Ca+Mg+Na)] and drought index [(CaO+MgO+Na<sub>2</sub>O+K<sub>2</sub>O)/(Fe<sub>2</sub>O<sub>3</sub>+MnO<sub>2</sub>)]. Additionally, the TOC content was determined by loss on ignition (LOI) when the samples were heated at 550 °C for 4 hours.

### 3.3 Chronology

In total, 32 OSL and <sup>14</sup>C samples were collected from the different lithological units of the typical sections, in order to establish the geochronological framework of the deposits. In detail, five <sup>14</sup>C samples from the weak palaeosol/palaeosols were analyzed at the Key Laboratory of Western China Environmental System (Ministry of Education), Lanzhou University, using organic matter as the dating material. The procedures used for <sup>14</sup>C dating were as described by Liu et al. (2014b). The <sup>14</sup>C dates were converted to calendar ages (Table 1) using the program Calib 7.04 based on the INTCAL 13 calibration (Reimer et al., 2013).

The OSL samples were obtained by hammering stainless-steel tubes horizontally into the freshly-cleaned vertical section, covered by a black plastic bag and sealed with opaque tape to avoid light exposure and moisture loss. In the laboratory, sediments at both ends of the cylinder were separated and used for water content and dose rate measurements, and the sample in the middle of the cylinder was used for equivalent dose (D<sub>e</sub>) measurement. In order to determine precisely the ages of the sediment samples, the OSL signals from quartz grains (4–11 μm) and the infrared-stimulated luminescence (IRSL) signals from K-feldspar grains (90–180 μm) were detected to estimate the D<sub>e</sub>, the analyses being conducted at the Institute of Hydrogeology and Environmental Geology, Chinese Academy of Geological Sciences and Cold and Arid Regions Environmental and Engineering Research Institute, Chinese Academy of Sciences, respectively. For the fine-grained quartz fraction, the samples were first treated with 30% HCl and 40% H<sub>2</sub>O<sub>2</sub> to remove carbonate and organic matter, then etched with 30% H<sub>2</sub>SiF<sub>6</sub> for five days to remove feldspars, the samples were finally rinsed with distilled water, and 4–11 μm quartz were extracted according to Stokes' Law and put into the oven for drying (40°C). All fine-grained samples were measured on a Daybreak 2200 automated OSL reader, equipped with a combined blue (470 ± 5 nm) and infrared (880 ± 80 nm) light emitting diode (LED) OSL unit, and a <sup>90</sup>Sr/<sup>90</sup>Y beta source (dose rate 0.084 Gy/s). The OSL signal from quartz was detected through one 3 mm thick Hoya U-340 filter. D<sub>e</sub> of the quartz sample was determined using a standard single aliquot regenerative-dose (SAR) protocol (Murray and Wintle, 2000).

**Table 1** <sup>14</sup>C results of the palaeosol/ weak palaeosol in the Gonghe Basin

Sample No.	Depth (cm)	Dated material	<sup>14</sup> C age (aBP)	Corrected age (2σ, Cal a BP)	Median age (Cal a BP)
LF-36	170–180	Organic matter	4765±30	5464–5588	5526
MGSW-1	70–80	Organic matter	1830±20	1714–1820	1767
DQW-1	200–220	Organic matter	4320±25	4841–4893	4867
DQW-2	300–320	Organic matter	7285±40	8015–8175	8095
DQW-3	370–380	Organic matter	7355±30	8038–8214	8126

For the coarse-grained fraction (90–180  $\mu\text{m}$ ) K-feldspar, the samples were first treated with 10% HCl and 20%  $\text{H}_2\text{O}_2$  to remove carbonate and organic matter, then sieved in water to obtain the 90–180  $\mu\text{m}$  size fraction. K-feldspars were then obtained by heavy liquid separation with densities of lower than  $2.58 \text{ g/cm}^3$ . The K-feldspar grains were etched with 10% HF for 40 min, and rinsed with 1 M HCl for 10 min and distilled water thereafter to remove fluorides. OSL signal measurements were carried out using an automated Risø TL/OSL-DA-15 reader, and the IRSL signal of K-feldspar was detected through combining one BG-39 filter with one Coring-759 filter. Laboratory irradiation was carried out using  $^{90}\text{Sr}/^{90}\text{Y}$  sources mounted within the reader with a dose rate of  $0.084 \text{ Gy/s}$  (Zhao et al., 2015). Using the SAR protocol, the IRSL signal observed at  $290^\circ\text{C}$  following a prior IR stimulation at  $50^\circ\text{C}$  was used for  $D_e$  measurement of K-feldspar, the detailed procedures being as described in Wang et al. (2019).

The U, Th and K contents of the samples were determined by Neutron Activation Analysis (NAA). All measurements were converted to alpha, beta and gamma dose rates according to the conversion factors of Aitken (1998). The dose rate from cosmic rays was calculated on the basis of burial depth, latitude, longitude and altitude of the samples (Prescott and Hutton, 1994). The water content was calculated as the ratio of water weight to the dried sample weight, an error of 5% being added to water content when the ages were being calculated. For calculations of the internal dose rate of K-feldspar fractions, a value of  $13 \pm 1\%$  was chosen as the K content (Zhao and Li, 2005). All measurement results and related parameters are presented in Fig. 3 and Table 2.

## 4 Results

### 4.1 Dating results and their reliability

A comparison of different dating approaches can provide a cross-check on the reliability of calculated ages. In this paper, the quartz OSL, K-feldspar IRSL and  $^{14}\text{C}$  dating approaches were applied to establish the age framework of palaeosol-aeolian sand sequences in the study region. Overall, Fig. 3 indicates that the results of OSL dating of quartz, K-feldspar  $\text{pIR}_{50}\text{IR}_{290}$  dating and  $^{14}\text{C}$  dating from different sections follow a good stratigraphic order, with the exception of sample LG 9, which yielded an apparent OSL age of  $8.69 \pm 0.41 \text{ ka}$  significantly younger than the ages of two overlying samples, i.e.,  $11.8 \pm 0.6 \text{ ka}$  for LG 8 and  $10.5 \pm 0.5 \text{ ka}$  for LG 7 (Table 2). This suggests that the age of LG 9 was underestimated. Four samples from the aeolian sand layer at the bottom of the LG section (LG7–10) have a roughly similar dose rate, however  $D_e$  value for LG 9 is clearly small compared to the other three samples from the same layer, i.e.,  $D_e$  value for LG 9 is  $22.01 \pm 0.73 \text{ Gy}$ , whereas all of the other samples have  $D_e$  values more than  $30.00 \text{ Gy}$ . This implies that the age underestimation for this sample is caused by the underestimation in its  $D_e$  value. In addition, the K-feldspar ages are in good agreement with the quartz ages from the HST and MGB sections, indicating that the quartz and K-feldspar fractions of the aeolian sand samples were fully bleached and that the results are reliable. The  $^{14}\text{C}$  results from interlaced palaeosol also show good consistency with the corresponding quartz OSL ages, which provides overall confidence in the dating reliability of the sections. Combined with lithological variations of different sections in the region, we found that

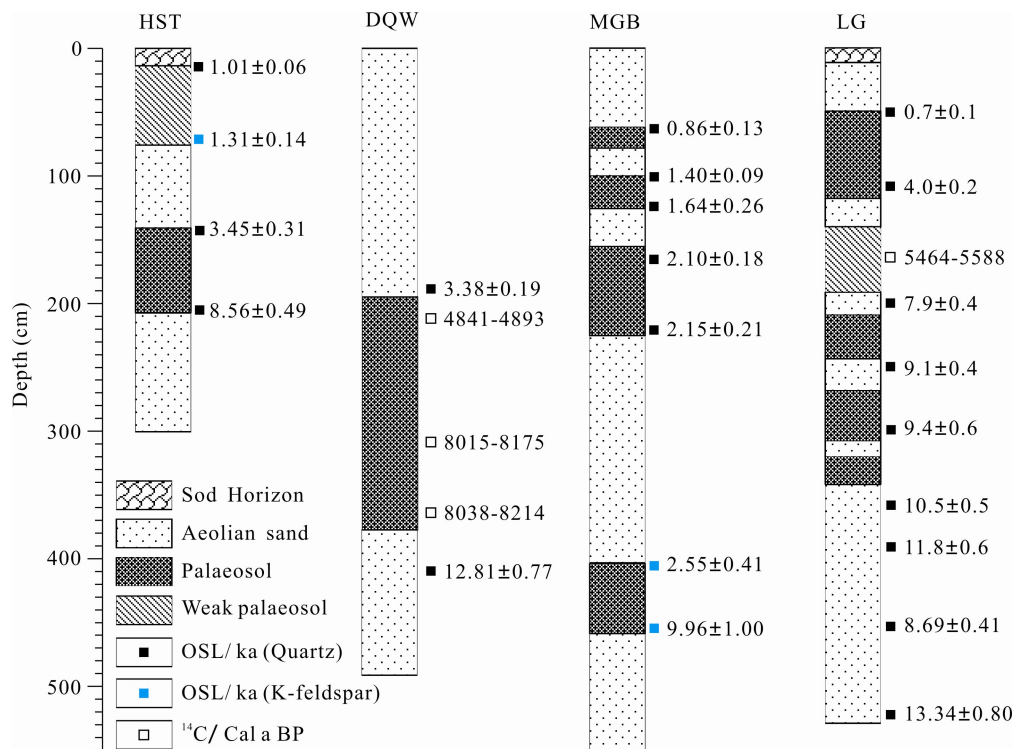


Fig. 3. OSL dating of quartz and K-feldspar and  $^{14}\text{C}$  ages from the typical sections.

**Table 2** The OSL dating and related parameters of aeolian deposits in the Gonghe Basin

Sample No.	Depth (cm)	Aliquots	Grain size ( $\mu\text{m}$ )	U (ppm)	Th (ppm)	K (%)	$D_e$ (Gy)	Dose rate (Gy/ka)	Water content (%)	OSL (ka)
LG1	45	8	4–11	1.30±0.07	6.02±0.19	1.35±0.05	1.89±0.16	2.62±0.10	1.83	0.7±0.1*
LG2	105	8	4–11	1.58±0.08	9.30±0.28	1.86±0.06	13.91±0.21	3.44±0.14	6.81	4.0±0.2*
LG4	200	8	4–11	1.60±0.08	6.85±0.22	1.75±0.06	24.85±0.57	3.14±0.12	3.84	7.9±0.4*
LG5	250	8	4–11	1.43±0.07	6.69±0.21	1.49±0.05	25.64±0.56	2.83±0.11	1.76	9.1±0.4*
LG6	300	8	4–11	1.63±0.08	7.91±0.25	1.58±0.06	28.84±1.56	3.08±0.12	3.47	9.4±0.6*
LG7	355	8	4–11	1.28±0.07	6.55±0.21	1.65±0.06	30.61±0.81	2.92±0.11	1.32	10.5±0.5*
LG8	390	8	4–11	0.97±0.06	5.81±0.20	1.47±0.05	30.80±0.98	2.55±0.10	0.82	11.8±0.6*
LG9	450	8	4–11	1.06	6.15	1.47	22.01±0.73	2.53±0.09	5.0	8.69±0.41
LG10	520	8	4–11	1.06	5.55	1.64	35.08±1.82	2.63±0.08	5.0	13.34±0.80
MGSW1	135	8	4–11	1.75±0.08	8.08±0.24	1.47±0.05	10.97±0.39	3.13±0.13	5.2	3.51±0.19
MGSW2	270	8	4–11	1.21±0.06	5.96±0.20	1.28±0.05	20.92±1.30	2.52±0.11	5.2	8.29±0.63
DQW1	200	8	4–11	1.68±0.08	7.50±0.24	1.56±0.05	10.60±0.41	3.13±0.13	4.2	3.38±0.19
DQW2	380	8	4–11	1.81±0.08	8.28±0.25	1.54±0.05	40.58±1.72	3.17±0.14	4.3	12.81±0.77
HST1	20	8	4–11	1.54±0.07	7.57±0.24	1.39±0.05	3.06±0.11	3.02±0.13	5.0	1.01±0.06
HST2	75	10	90–180	1.38±0.07	7.29±0.23	1.50±0.05	4.15±0.28	3.18±0.26	4.3	1.31±0.14
HST3	170	8	4–11	1.70±0.08	9.06±0.26	1.57±0.05	11.53±0.93	3.34±0.14	2.9	3.45±0.31
HST4	210	8	4–11	1.55±0.07	7.20±0.23	1.37±0.05	24.67±0.96	2.88±0.12	2.8	8.56±0.49
MGB1	60	8	4–11	1.69±0.08	6.80±0.22	1.40±0.05	2.57±0.37	3.01±0.13	0.6	0.86±0.13
MGB2	100	8	4–11	1.62±0.07	6.47±0.21	1.42±0.05	4.15±0.19	2.97±0.12	2.2	1.40±0.09
MGB3	125	8	4–11	1.65±0.08	7.33±0.23	1.38±0.05	4.93±0.76	3.01±0.13	0.8	1.64±0.26
MGB4	160	8	4–11	1.53±0.07	6.75±0.22	1.41±0.05	6.16±0.46	2.94±0.13	0.2	2.10±0.18
MGB5	235	8	4–11	1.25±0.06	5.80±0.20	1.41±0.05	5.80±0.52	2.70±0.12	1.3	2.15±0.21
MGB6	405	11	90–180	1.29±0.07	6.75±0.22	1.37±0.05	7.06±0.94	2.77±0.24	9.8	2.55±0.41
MGB7	430	12	90–180	1.05±0.05	4.72±0.16	1.22±0.04	25.91±1.01	2.60±0.24	2.5	9.96±1.00
SYD1	60	8	4–11	1.40±0.07	6.69±0.21	1.30±0.05	12.97±0.19	2.95±0.12	1.36	4.40±0.19
SYD2	120	8	4–11	1.45±0.07	8.13±0.24	1.39±0.05	15.69±0.19	2.95±0.13	3.04	5.32±0.24
SYD3	255	8	4–11	1.24±0.07	6.17±0.20	1.28±0.05	23.01±0.58	2.57±0.11	1.25	8.94±0.44

\*These results were first reported by Liu et al. (2013)

aeolian sands are widely accumulated at the interval of 13–9 ka in the eastern and middle of the Gonghe Basin. At approximately 9–8 ka, aeolian sands were gradually replaced by palaeosols until ~4–3 ka. Thereafter, the stratum presented the frequent alternation of the palaeosol/weak palaeosol and aeolian sand, although the dating results vary from site to site (Fig. 3).

#### 4.2 Geochemical parameter characteristics and their palaeoclimatic significance

Geochemical parameters were used to discriminate the dry-wet variations in aeolian deposits since the Late Quaternary across the Asian summer monsoonal boundary belt of northern China (Qiang et al., 2010; Lu et al., 2011; Liu et al., 2015). Specifically, the eluviation coefficient was used to reflect the residual status of sediments under the weathering process, which is closely related to dry-wet fluctuations of the climate (Jin et al., 2004). Owing to the stronger chemical activity of CaO, MgO, Na<sub>2</sub>O and K<sub>2</sub>O, they are easily leached in response to enhancement of temperature and precipitation, whereas Al<sub>2</sub>O<sub>3</sub> and Fe<sub>2</sub>O<sub>3</sub> are relatively stable due to their inactive geochemical properties compared to CaO, MgO, Na<sub>2</sub>O and K<sub>2</sub>O. Hence, this coefficient decreases with aridification, and vice versa. Likewise, based on the differentiation of the geochemical properties of some elements, i.e. Al, Fe, Mn and Na, K, Ca, the humidity index (C) and drought index (Re) are also regarded as indicators for distinguishing dry-wet variations. When the climate becomes dry, K, Na, Ca and Mg contents increase while Al, Fe, and Mn contents decrease (Jin et al., 2004; An et al., 2006; Liu et al., 2015). Hence, the increased C-value implies a relatively wet environment, while increased Re is usually related to an

arid environment. The Rb/Sr ratio was used as the regional moisture proxy ascribed to differential geochemical properties. Rb is mainly dispersed in K-containing minerals such as muscovite and K-feldspar, which is readily adsorbed during the weathering process due to its higher ionic radius. In contrast, Sr has a preference for Ca-containing minerals such as plagioclase, amphibole, pyroxene and carbonate minerals. During the weathering process under earth surface conditions, the former are usually more steady than the latter, which results in fractionation between Rb and Sr (Chen et al., 1999). Aeolian deposits have a higher Sr and lower Rb content, and therefore a lower Rb/Sr ratio emerged in the aeolian sand or loess layer, but inversely in the palaeosol due to the relatively wet climate (Liu et al., 2014c; Ding et al., 2019).

As presented in Fig. 4, the eluviation coefficients of the palaeosol/weak palaeosol were clearly higher than that of the aeolian sand in the different sections. These variations closely resemble that of the Rb/Sr, moisture index and TOC content in different lithological units, whereas they varied inversely with the drought index in the section. Combined with sedimentary lithology and dating results, we found that the DQW and LG sections exhibited a relatively low eluviation coefficient, Rb/Sr, and a moisture index around 12.81–8.2 ka and 13.34–9.1 ka, whereas they approached the maximum of the sections around 8.2–3.38 ka and 9.1–4.0 ka with a reduced drought index and increased TOC content. These variations are consistent with that of geochemical indicators in the HST and MGB sections, which also presented maximum values for the eluviation coefficient, Rb/Sr, moisture index and TOC content around 8.56–3.45 ka and 9.96–2.55 ka. Since then,

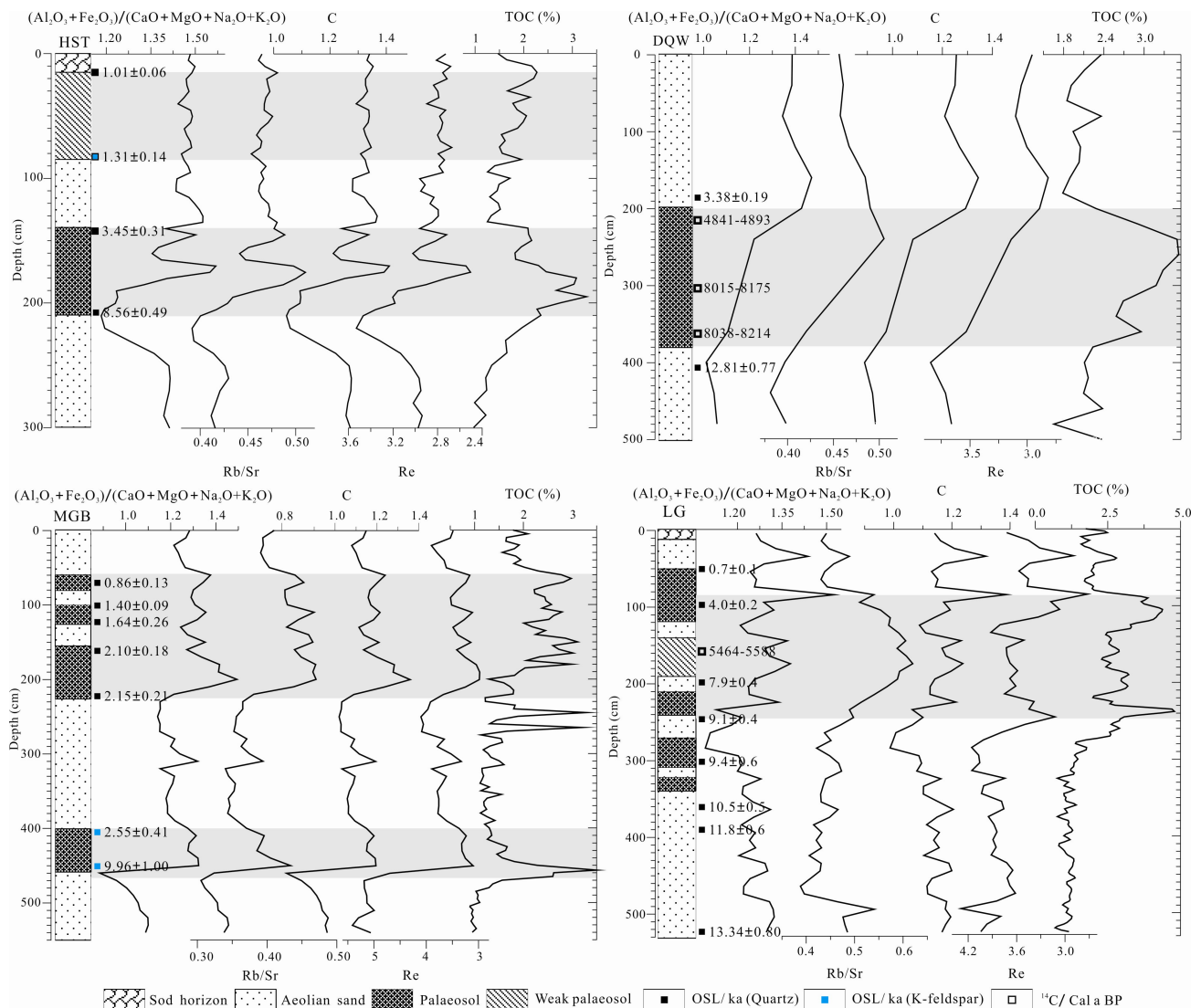


Fig. 4. Geochemical parameters indicate effective moisture variations inferred from sections in this study.

the geochemical parameters presented diverse variations due to the frequent alternation of the aeolian sand-palaeosol/weak palaeosol between different sections. For example, the eluviation coefficient, Rb/Sr, moisture index and TOC content gradually declined in the LG and DQW sections. In contrast, these indicators remained high in the MGB and HST sections. In particular, the Rb/Sr and TOC content of the MGB section were apparently high around 2.15–0.86 ka, although there were frequent fluctuations.

## 5 Discussions

### 5.1 Holocene effective moisture variation inferred from aeolian deposits in the Gonghe Basin

Based on dating results and proxy variations of four typical aeolian deposits in the Gonghe Basin, the palaeoclimatic evolution framework can be established as follows:

#### Late glacial-Early Holocene

OSL dating results reveal that well-sorted aeolian sand accumulated around  $12.81 \pm 0.77$  ka and  $13.34 \pm 0.80$  ka–

$10.5 \pm 0.5$  ka in the eastern and middle of the Gonghe Basin, which indicates a dry or low effective moisture condition around 13–10 ka. Specifically, the eluviation coefficient, Rb/Sr and moisture index remain the lowest with an evident high drought index in the DQW section of the eastern Gonghe Basin, which illustrates an arid climatic condition. The low but fluctuating TOC content also reflect limited vegetation at this interval (Fig. 4). The contemporaneous climate background was also evidenced by geochemical proxies from the LG sections of the middle Gonghe Basin, e.g., minimum Rb/Sr and TOC contents and a prominent high drought index. Similarly, the ages of the buried aeolian sands had  $> 8.56 \pm 0.49$  ka and  $9.96 \pm 1.00$  ka in the southern and northern Muge Sands, accompanied with a sharply decreased moisture index and Rb/Sr ratios and a persistently high drought index from the HST and MGB sections (Fig. 4). Thus, the aforementioned evidence demonstrates a very low moisture regime within an active desert environment.

#### Middle Holocene

The aeolian sands were replaced by the palaeosol/weak

palaeosols since 9–8 ka in the Gonghe Basin, i.e., OSL ages indicate that palaeosols were developed in 8.56–3.45 ka, 8.2–4.8 cal ka, 9.96–2.55 ka in the eastern Gonghe Basin, which indicates that the desert was fixed in the middle Holocene (Fig. 4). In detail, the eluviation coefficient, Rb/Sr and moisture index of the HST and MGB sections approached a maximum, although several fluctuations existed during this interval. The TOC contents also gradually increased, accompanied by a sharply reduced drought index. In the LG section, moisture proxies, including the eluviation coefficient and C value, continuously improved, and Rb/Sr and TOC contents show the highest values, which mirrored the conspicuous enhancement of the regional effective moisture and favorable vegetation cover in the Gonghe Basin during that time.

#### Late Holocene

The alternation of aeolian sand-palaeosol/weak palaeosol from multiple sections indicates that the desert environment had clearly deteriorated due to the developed aeolian sand since 4–3 ka. Aeolian sand dominated the deposits in the DQW section in the eastern Gonghe Basin around 3.38 ka, together with a reduced Rb/Sr ratio and TOC content (Fig. 4). The weakly-developed and thin palaeosol replaced the ash black palaeosol of high TOC content in the HST, MGB and LG sections, which overall reflects the decreased moisture and weak vegetation conditions since the late Holocene. It is worth noting that several short-lived relatively wet intervals still occurred in this arid context, i.e., the weak palaeosol and palaeosol developed around 1.3–1.0 ka, 2.15–2.10 ka, 1.64–1.40 ka and 0.86 ka in the southern and northern Muge Sands. The related proxies from these sections also demonstrate that the regional moisture was briefly enhanced, which is further evidenced by variations of the eluviation coefficient, Rb/Sr and TOC content from the MGB section (Fig. 4). These details illustrate that although the regional moisture condition was relatively arid since the Late Holocene, relatively wet events still occurred.

#### 5.2 Comparison of the Holocene moisture variation in the Gonghe Basin and adjacent regions

The framework of Holocene effective moisture variation was established based on dozens of OSL ages and sequences of geochemical parameters from four representative geological sections in the Gonghe Basin. This generally indicates that an arid climate dominated the region during the early Holocene, and that optimum moisture occurred in the middle Holocene. Afterwards, the region became dry but with several wet intervals since the late Holocene. Massive OSL results also support stronger dune activity forced by low effective moisture from the late glacial to early Holocene in the Gonghe Basin and its adjacent regions. Liu et al. (2013a) and Qiang et al. (2013b) reported that aeolian sands were extensively developed in the northern Muge Sands and middle Gonghe Basin, 11.2±0.6 ka and 11.8–11.0 ka, respectively, which roughly correspond to the cold interval of the Younger Dryas (YD). Recently, <sup>14</sup>C and OSL results demonstrated that aeolian sand occupied the eastern and northern Muge Sands owing to the dry climate

at that time (Stauch et al., 2018; Hu et al., 2019). Similarly, contemporaneous aeolian sands were documented in the eastern Qinghai Lake Basin (Lu et al., 2015), Qaidam Basin desert (Yu and Lai, 2014) and the headwaters of the Daotang River (Liu et al., 2012) with coarse grain size, lower TOC content and magnetic susceptibility. Based on comprehensive analysis of OSL ages and sedimentary lithology from the Gonghe Basin, we discovered that widespread aeolian sand accumulation lasted until 12–10 ka, with dune fields remaining mobile (Figs. 5 and 6a).

Around 10–9 ka, a weak palaeosol/palaeosol gradually developed in the eastern Gonghe Basin, confirming that the regional climate tended to be relatively humid. The MGB section revealed that the palaeosol formed since around 9.96 ka with a high TOC content and the lowest drought index, which is synchronous with that of the palaeosol in the LG profile in the middle of the Gonghe Basin. Similarly, a palaeosol was also developed during 10–8 ka in the southern Muge Sands (Fig. 2f), which is also indicated by the OSL and <sup>14</sup>C age of the palaeosol in the eastern Qinghai Lake (Liu et al., 2012; Lu et al., 2011, 2015; Ding et al., 2019) and Qaidam Basin (Yu and Lai, 2014). At the same time, analysis of different proxies in lake sediments, i.e., Gengga, Qinghai and Chaka Salt lakes, illustrates that a humid climate led to persistently high lake levels (Liu et al., 2008; An et al., 2012; Qiang et al., 2013a), which are regarded as the early and middle Holocene climate optimum period. However, records of aeolian deposits around the northeastern QTP demonstrate that aeolian sand still accumulated during that interval, e.g., the SYD and MGTA sections show that aeolian sand developed at 9.7–7.8 ka and 8.94±0.44 ka in the western and central northern Muge Sands (Fig. 2c). Similar sand deposits were also found at eastern and western Qinghai Lake and the eastern Qaidam Basin desert during the 9–7 ka interval (Liu et al., 2012; Lu et al., 2015). In summary, we consider that the climate of the early Holocene was relatively dry, although obviously ameliorated compared with 13–10 ka (Fig. 6b).

In the middle Holocene (9–4/3 ka), aeolian sand was replaced by palaeosol, which verifies an optimum wet environment in the Gonghe Basin. Overall, the dune field was fixed and semi-fixed at 9–3 ka, especially in the Muge Sands. For example, in the eastern Gonghe Basin, palaeosol ages are 8.56–3.45 ka, 8.2–4.8 cal ka BP and 9.96–2.55 ka from the HST, DQW and MGB sections, respectively. In the middle and western Gonghe Basin, palaeosol ages are 7.8–5.7 ka, 8.0–4.8 cal ka BP, 8.1–2.5 ka and 9–4 ka from the MGTA, MS, TGM and LG sections, respectively. In the western Gonghe Basin, pollen-based reconstruction from Dalian Lake indicates that the vegetation was dominated by grassland and high covered desert steppe at 9–4 ka (Cheng et al., 2013). The quantitative reconstruction of regional precipitation also concluded that the highest moisture occurred in the middle Holocene (Li et al., 2017), which is consistent with geochemical results and pollen analysis in slope sediments of the eastern Gonghe Basin (Liu et al., 2014b; Miao et al., 2015). In the Qinghai Lake Basin, the palaeosol presented an optimal developed period during 8–4 cal ka BP,

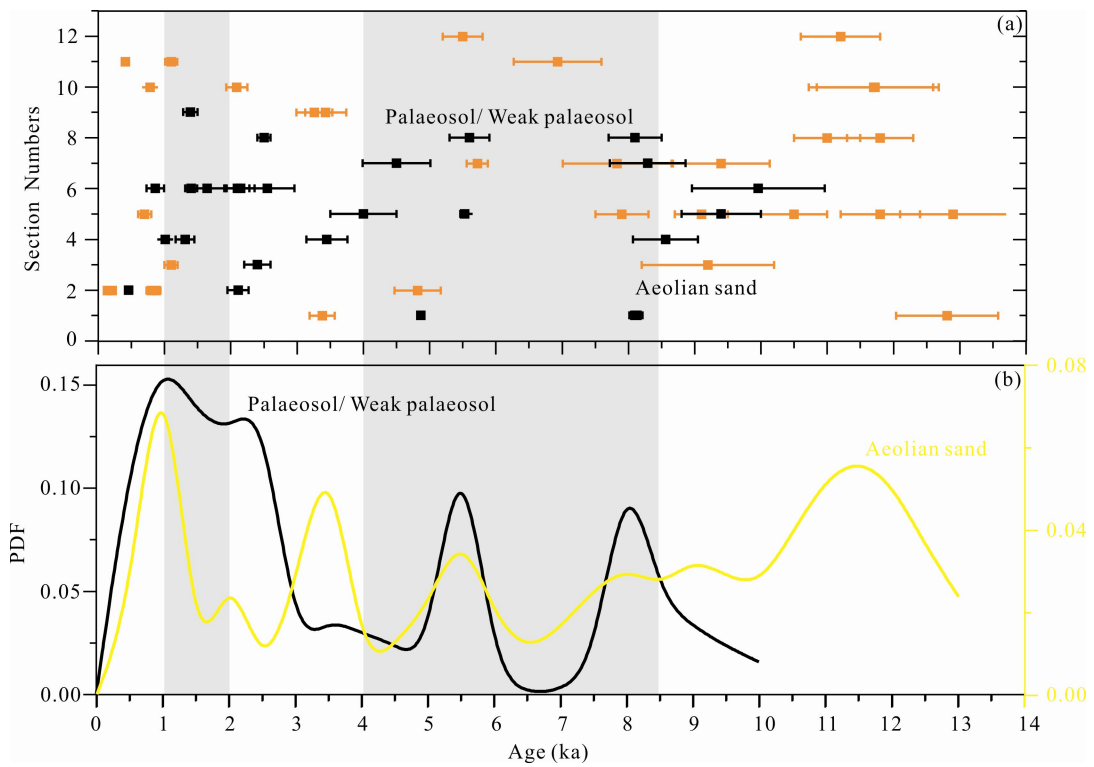


Fig. 5. OSL ages and Probability Density Function (PDF) of the aeolian sand and palaeosol in the Gonghe Basin dune field, northeastern QTP.

(a) Synthesized OSL ages derived from the Gonghe Basin dune field; (b) PDF curve of aeolian sand and palaeosol (Liu et al., 2013a; Qiang et al., 2016; Stauch et al., 2018; Tian et al., 2020), the shadows in the figure illustrated the period of paleosol development.

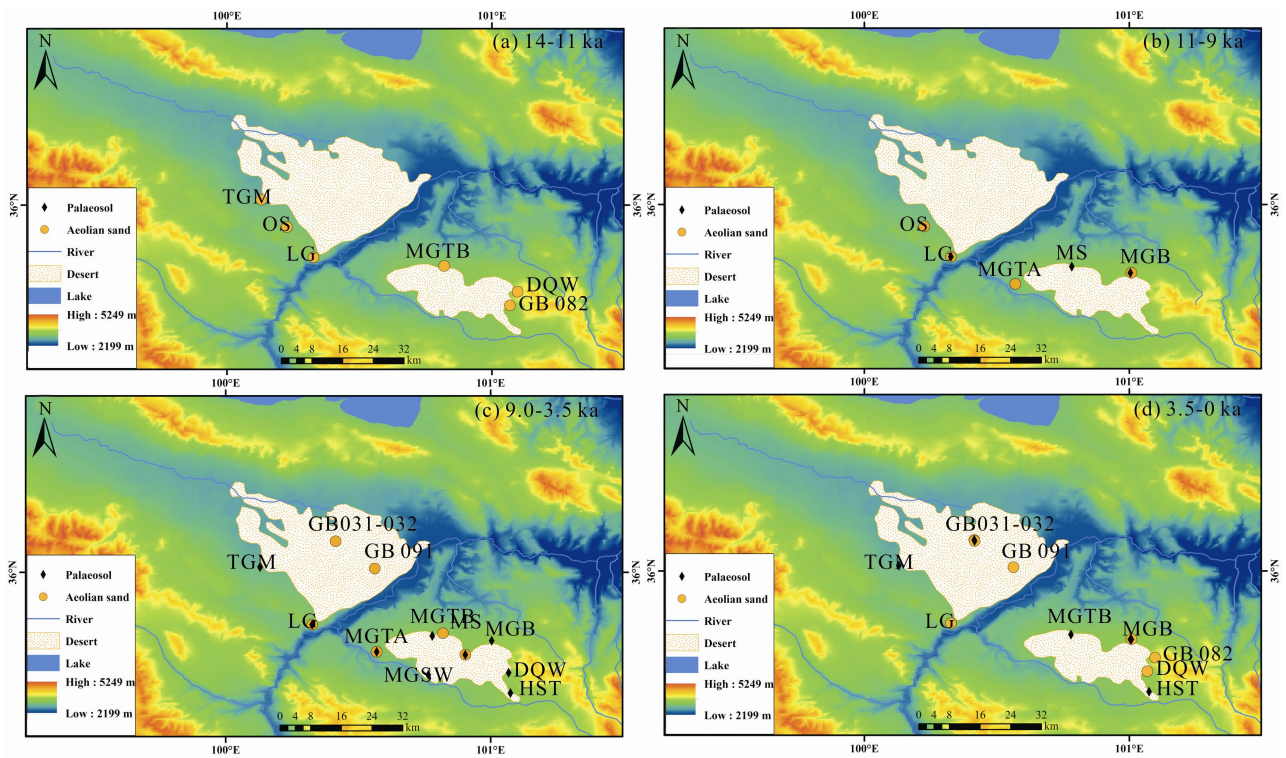


Fig. 6. Holocene moisture variation inferred from dating results and sediment facies in the Gonghe Basin, northeastern QTP.

accompanied by enhanced geochemical weathering, Rb/Sr and TOC content (Lu et al., 2015; Ding et al., 2019).

Nevertheless, episodes of aeolian activity and reduced moisture still emerged around 5.5 ka (Qiang et al., 2013b;

Liu et al., 2013a, Figs. 5 and 6c), which is probably correlated, on a global scale, with climatic deterioration of the middle Holocene.

Subsequently, the regional climate gradually became dry since the late Holocene, as demonstrated by the reemergence of aeolian sand and the alternation of aeolian sand-weak palaeosol/palaeosol in the Gonghe Basin (Stauch et al., 2018; Hu et al., 2019, Fig. 6d). This tendency was recorded in adjacent regions, i.e., the palaeosol was gradually replaced by aeolian sand and loess deposits in the eastern Qinghai Lake Basin, along with decreased magnetic susceptibility, TOC content and coarse grain size and weak geochemical weathering (Lu et al., 2011, 2015; Ding et al., 2019). In the eastern Qaidam Basin desert, the stratum also recorded similar characteristics, reflecting arid surroundings since the late Holocene (Yu and Lai, 2014). The biological community was dominated by desert steppe, mainly *Chenopodiaceae*, *Artemisia* and *Poaceae*, with a decreased size of Dalian Lake since 3.9 cal ka BP (Cheng et al., 2013). Pollen concentration and TOC content decreased sharply, while *Artemisia* expanded around 4.5 cal ka BP at Qinghai Lake, indicating that the climate evolved to be cold and arid (Shen et al., 2005). Gengga Lake depth began to reduce and the salinity of Chaka Salt Lake sharply increased since the late Holocene (Liu et al., 2008; Qiang et al., 2013a). It is worth noting that relatively wet intervals have been discovered in the Gonghe Basin around 2 ka, according to variations of geochemical parameters and sedimentary facies. The OSL ages and environmental proxies illustrate relatively wet intervals around 2.1 ka and 1.6–1.4 ka in the MGB section (Fig. 4), which indicate that the climate is analogous to that of the middle Holocene. Since then, the regional climate became very dry along with aeolian activity, as revealed by multi-proxies of the LG and MGB sections.

### 5.3 Holocene moisture variation in the Gonghe Basin and its response to the Asian monsoon

The Late Quaternary moisture variation in northeastern QTP was mainly controlled by different atmospheric circulations on a different geological time scale, i.e., the Asian summer and winter monsoons, and westerlies (An et al., 2012). According to modern climatic observations, abundant precipitation occurs as the moisture source in this region is brought by an enhanced Asian summer monsoon, forced by solar insolation (Dong et al., 1993; Wu et al., 2016). The regional moisture variation is closely related with the balance of potential evaporation and precipitation capacity (Qiang et al., 2013b). At present, there are two main different conceptual models which explain the Holocene climatic change and its possible mechanisms: oxygen isotopes (Liu et al., 2007), pollen (Shen et al., 2005), authigenic carbonate (Liu et al., 2014) and geochemical parameters (Jin et al., 2016) of Qinghai Lake, plant fossils of Gengga Lake (Qiang et al., 2013a) and OSL results of aeolian deposits in the Qaidam Basin (Yu and Lai, 2014) demonstrate that regional moisture variations were mainly followed by solar insolation and maximum humidity, which occurred in the early and middle Holocene of northeastern QTP. In comparison, multi-proxy records of the aeolian sand/loess-palaeosol sequences around Qinghai Lake and Gonghe Basin (Lu et al., 2011, 2015; Qiang et al., 2013b; Liu et al., 2014b; Ding et al., 2019) indicate that optimal moisture occurred in the middle to even late Holocene, which is probably attributable to an increased Asian summer monsoon and related balance of evaporation–precipitation. We therefore compared our record to possible influencing factors, in order to ascertain the pattern of the regional effective moisture (Fig. 7). Figure 7g illustrates the framework of the Holocene moisture variation in the Gonghe Basin, through the standardized and synthesized Rb/Sr ratio from direct OSL data of four representative sections in this

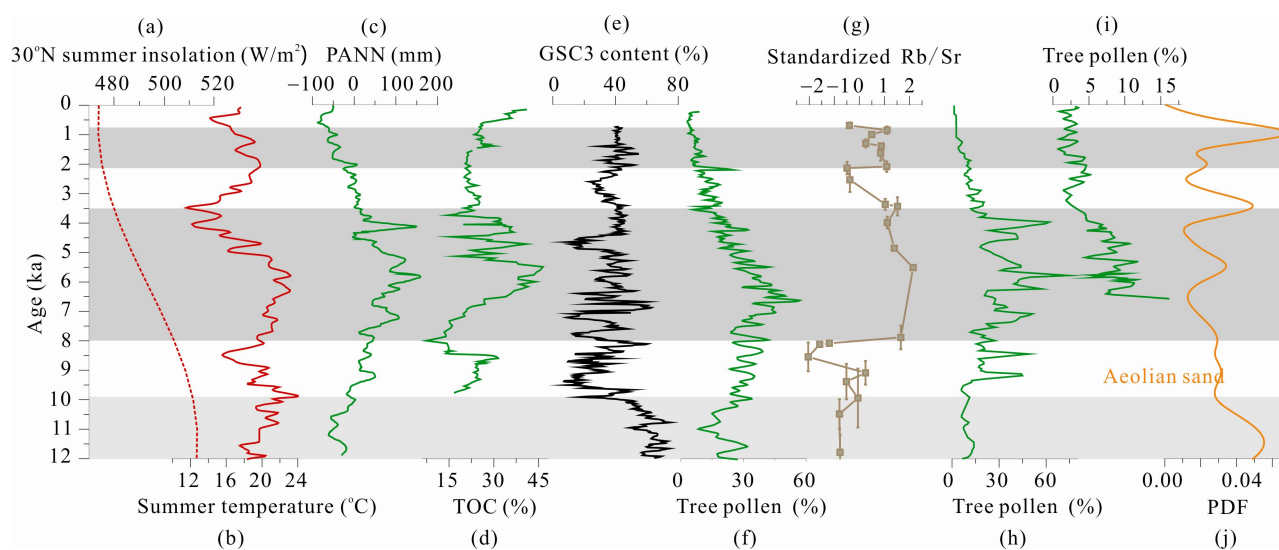


Fig. 7. Possible influencing factors for the Holocene moisture variation in the Gonghe Basin, northeastern QTP.

(a) 30°N Solar insolation (Berger and Loutter, 1991); (b) Summer temperature inferred from Qinghai Lake (Hou et al., 2016); (c) PANN based on lakes Dalianhai and Qinghai (Li et al., 2017); (d) Moisture variation in the eastern Gonghe Basin (Liu et al., 2014b); (e) Holocene winter monsoonal evolution (Liu et al., 2018); (f) Tree pollen of Qinghai Lake (Shen et al., 2005); (g) Rb/Sr record of aeolian deposits in the Gonghe Basin (this study); (h) Tree pollen of Dalianhai Lake (Cheng et al., 2013); (i) Tree pollen of Genggahai Lake (Liu et al., 2016); (j) Aeolian activity based on the PDF of OSL dating and aeolian sand in the Gonghe Basin (Liu et al., 2013a; Qiang et al., 2016; Stauch et al., 2018; Hu et al., 2019 and this study).

study, which indicate that effective moisture is the lowest in the early Holocene (12–9/8 ka), approached a maximum in the middle Holocene (9–4 ka), and became relatively low in the Late Holocene.

In the late glacial-early Holocene, the highest summer insolation at 30°N resulted in apparently high summer temperatures and potential evaporation (Fig. 7a–b; Berger and Loutre, 1991; Hou et al., 2016). This is supported by very low  $P_{ANN}$ , and tree pollen concentrations in lake and peat archives of western and eastern Gonghe Basin (Fig. 7c–d, h; Li et al., 2017; Cheng et al., 2013; Miao et al., 2015). Mason et al. (2009) emphasized that dry conditions at the desert margin of Northern China during the early Holocene could be explained through a dynamic link between enhanced diabatic heating in the core region of the strengthened monsoon and increased subsidence in drylands to the north, combined with high evapotranspiration rates due to high summer temperatures. Recently, pollen analysis of lakes Gonghai and Dali from northern and northeastern China (Cheng et al., 2015a; Wen et al., 2017) mirrored that of the East Asian summer monsoon, which did not intensify until ~8000 cal BP, owing to the existence of an intense winter monsoon, caused by remnants of Northern Hemisphere ice sheets (Dyke, 2004). This is coincident with stronger winter monsoon records from northwestern China (Qiang et al., 2010; Liu et al., 2018) and the Gonghe Basin (Liu et al., 2013b), which led to intense aeolian activity in northeastern QTP, especially in the middle and eastern Gonghe Basin (Fig. 7e and j, Qiang et al., 2013b; Chen et al., 2016a; Liu et al., 2018; Stauch, 2018). We therefore conclude that effective moisture maintained low levels until 9–8 ka, which can partly be attributed to high evaporation and stronger winter monsoons (Fig. 7).

Since 9–8 ka, regional effective moisture was clearly elevated, as shown by increased  $P_{ANN}$  (Fig. 7c), tree pollen in lakes Dalian, Gengga and Qinghai (Fig. 7f, h–i) and the Rb/Sr ratio of the aeolian deposit (Fig. 7g) in northeastern QTP. Meanwhile, summer temperatures and Asian winter monsoons sharply dropped, compared to 12–8 ka, although there were frequent fluctuations. Lu et al. (2005) found that the peak of the summer monsoon of northern China had a lag response of several thousand years with summer insolation, and high summer monsoon rainfall began around 8–7 ka. Mason et al. (2009) also concluded that lower temperatures and reduced evapotranspiration led to stabilized aeolian sand and even palaeosol development with increased vegetation after 8 ka. Different proxies and dating results from aeolian deposits of dune fields in northern China also support a stronger Asian summer monsoon during the Middle Holocene, along with dense vegetation coverage and a contracted desert area (Sun et al., 2006; Zeng et al., 2018; Yang et al., 2010, 2013; Liu et al., 2014c). Afterwards, the effective moisture apparently became low compared with the middle Holocene in the studied region, which is accompanied with declining summer temperatures, monsoon precipitation and vegetation coverage (Fig. 7a–c, f, h–i). Correspondingly, the palaeosols were replaced with aeolian sand and the peak of strong dune activity took place around 3.5 ka and 1.5 ka (Fig. 7j). It is worth

noting that the relatively humid interval was recorded around 2–1 ka, which is closely related to the ameliorative climate condition around northeastern QTP in the past 2 ka (Yang et al., 2014; Stauch, 2016). Overall, effective moisture variation is closely related to the Asian summer monsoonal strength and therefore a balance of evaporation-precipitation in the Gonghe Basin, which at least presented an apparent monsoon model in the Holocene.

## 6 Conclusions

The geochemical analysis of aeolian sand-palaeosol sequences from the Gonghe Basin, northeastern QTP, combined with OSL dating, reveals a Holocene effective moisture variation framework pattern in an intermontane basin in the semi-arid area, in western China.

(1) A dry environment dominated the region during the early Holocene, which is accompanied by massive accumulation of aeolian sand, the low Rb/Sr ratio and sparse vegetation. Since 9–8 ka, regional effective moisture was clearly enhanced, along with increased vegetation as well as palaeosol development. The climate tended to be relatively dry after 4–3 ka, along with a transient humid interval around 2–1 ka.

(2) Geochemical evidence indicates that the dry early Holocene probably can be attributed to the high evaporation triggered by solar insolation, as well as the strong winter monsoon forced by remnant ice sheet, whereas the shift of humid-dry was closely linked to the Asian summer monsoonal strength and therefore balance of the evaporation-precipitation in the middle-late Holocene.

(3) In summary, the framework pattern of the Holocene effective moisture variation is characterized as the ‘monsoon model’ in a closed intermontane arid and semi-arid basin near the western Asian monsoonal limit of China.

## Acknowledgements

This study was supported by the Strategic Priority Research Program of Chinese Academy of Sciences, Pan-Third Pole Environment Study for a Green Silk Road (Grant No. XDA 2009000001) and the National Natural Science Foundation of China (Grants No. 41977393 and 41671204). We are grateful to the reviewers and editor for their valuable suggestions for improving the paper.

Manuscript received Feb. 21, 2020

accepted Apr. 2, 2020

associate EIC: CHEN Fahu

edited by FEI Hongcai

## References

- Aitken, M.J., 1998. *An Introduction to Optical Dating*. Oxford, UK: Oxford University Press.
- An, C.B., Feng, Z.D., and Barton, L., 2006. Dry or humid? Mid-Holocene humidity changes in arid and semi-arid China. *Quaternary Sciences Reviews*, 25: 351–361.
- An, Z.S., Colman, S.M., Zhou, W.J., Li, X.Q., Brown, E.T., Timothy, Jull.J.A., Cai, Y.J., Huang, Y.S., Lu, X.F., Chang, H., Song, Y.G., Sun, Y.B., Xu, H., Liu, W.G., Jin, Z.D., Liu, X.D., Cheng, P., Liu, Y., Ai, L., Li, X.Z., Liu X.J., Yan, L.B.,

- Shi, Z.G., Wang, X.L., Wu, F., Qiang, X.K., Dong, J.B., Lu, F.Y., and Xu, X.W., 2012. Interplay between the Westerlies and Asian monsoon recorded in Lake Qinghai sediments since 32 ka. *Scientific Reports*, 2: 619.
- Berger, A., and Loutre, M.F., 1991. Insolation values for the climate of the last 10 million years. *Quaternary Science Reviews*, 10: 297–317.
- Bryson, A.J., 1986. Airstream Climatology of Asia. In: *Proceedings of International Symposium on the Qinghai-Xizang Plateau and Mountain Meteorology*. American Meteorological Society, 604–617.
- Chen, F., Wu, D., Chen, J., Zhou, A., Yu, J., Shen, J., Wang, S., and Huang, X., 2016a. Holocene moisture and East Asian summer monsoon evolution in the northeastern Tibetan Plateau recorded by Lake Qinghai and its environs: A review of conflicting proxies. *Quaternary Science Reviews*, 154: 111–129.
- Chen, F.H., Xu, Q.H., Chen, J.H., Birks, H.J., Liu, J.B., Zhang, S.R., Jin, L.Y., An, C.B., Telford, R.J., Cao, X.Y., Wang, Z.L., Zhang, X.J., Selvaraj, K., Lu, H.Y., Li, Y.C., Zheng, Z., Wang, H.P., Zhou, A.F., Dong, G.H., Zhang, J.W., Huang, X.Z., Bloemendal, J., and Rao, Z.G., 2015. East Asian summer monsoon precipitation variability since the last deglaciation. *Scientific Reports*, 5: 11186.
- Chen, J., An, Z.S., Wang, Y.J., Ji, J.F., Chen, Y., and Lu, H.Y., 1999. Distribution of Rb and Sr in the Luochuan loess-paleosol sequence of China during the last 800 ka: implications for paleomonsoon variations. *Science China Earth Sciences*, 42 (3): 225–232.
- Chen, J.H., Rao, Z.G., Liu, J.B., Huang, W., Feng, S., Dong, G.H., Hu, Y., Xu, Q.H., and Chen, F.H., 2016b. On the timing of the East Asian summer monsoon maximum during the Holocene—Does the speleothem oxygen isotope record reflect monsoon rainfall variability? *Science China Earth Sciences*, 59: 2328–2338.
- Cheng, B., Chen, F.H., and Zhang, J.W., 2013. Palaeovegetational and palaeoenvironmental changes since the last deglacial in Gonghe Basin, northeast Tibetan Plateau. *Journal of Geographical Sciences*, 23 (1): 136–146.
- De Baar, W., De Jong, J.T.M., Bakker, D.C.E., Bettina, M.L., Cornelis, V., Bathmann, U., and Smetacek, V., 1995. Importance of iron for plankton blooms and carbon dioxide drawdown in the Southern Ocean. *Nature*, 373: 412–415.
- Ding, Z.Y., Lu, R.J., Lyu, Z.Q., and Liu, X.K., 2019. Geochemical characteristics of Holocene aeolian deposits east of Qinghai Lake, China, and their paleoclimatic implications. *Science of the Total Environment*, 692: 917–929.
- Dong, G.R., Gao, S.Y., and Jin, J., 1993. *Desertification and Its Control in Gonghe Basin of Qinghai Province*. Beijing: Science Press, 10–33 (in Chinese with English Abstract).
- Dyke, A.S., 2004. An outline of North American deglaciation with emphasis on central and northern Canada. *Development Quaternary Sciences*, 2(B): 373–424.
- Fan, Y.X., Chen, X.L., Fan, T.L., Jin, M., Liu, J.B., and Chen, F.H., 2013. Sedimentary and OSL dating evidence for the development of the present Hobq desert landscape, northern China. *Science China Earth Sciences*, 56: 2037–2044.
- Fan, Y.X., Zhang, F., Zhang, F., Liu, W.H., Chen, X.L., Fan, T.L., Wang, Y.D., Chen, F.H., and Lai, Z.P., 2016. History and mechanisms for the expansion of the Badain Jaran Desert, northern China since 20 ka: Geological and luminescence chronological evidence. *The Holocene*, 26(4): 532–548.
- Gao, S.Y., Cheng, W.N., Jin, H.L., Dong, G.R., Li, B.S., Yang, G.S., Liu, Li.Y., Guan, Y.Z., Sun, Z., and Jin, J., 1993. Preliminary study on the desert changes at the northwest edge of China. *Science China Chemistry*, 23(2): 203–208. (in Chinese)
- Gao, Y.X., Xu, S.Y., Guo, Q.Y., and Zhang, M.L., 1962. Monsoon zone and monsoon climate in China, in: Gao, Y.X., (eds.), *Some Problems on East Asia Monsoon*. Beijing: Science Press, 49–59.
- Herzschuh, U., Borkowski, J., Schewe, J., Mischke, S., and Tian, F., 2014. Moisture-advection feedback supports strong early-to-mid Holocene monsoon climate on the eastern Tibetan Plateau as inferred from a pollen-based reconstruction. *Palaeogeography, Palaeoclimatology, Palaeoecology*, 402: 44–54.
- Hou, J.Z., Huang, Y.S., Zhao, J.T., Liu, Z.H., Colman, S., and An, Z.S., 2016. Large Holocene summer temperature oscillations and impact on the peopling of the northeastern Tibetan Plateau. *Geophysical Research Letters*, 43: 1323–1330.
- Hu, M.J., Feng, S.Q., and Li, X.F., 2019. The environmental evolution of the Gonghe Basin since the 12 ka revealed by magnetic susceptibility. *Journal of Stratigraphy*, 43(1): 101–108 (in Chinese with English Abstract).
- Jiang, K., Wang, X.S., and Mei, S., 2018. The first loess-based paleoclimatic reconstruction over the last Interglacial-Glacial cycle in the Hunshandake Sandy Land. *Acta Geologica Sinica (English Edition)*, 92(3): 1285–1286.
- Jin, H.L., Su, Z.Z., Sun, L.Y., Sun, Z., Zhang, H., and Jin, L.Y., 2004. Holocene climatic change in Hunshandake desert. *Chinese Sciences Bulletin*, 49(16): 1730–1735.
- Jin, Z.D., An, Z.S., Yu, J.M., Li, F.C., and Zhang, F., 2016. Lake Qinghai sediment geochemistry linked to hydroclimate variability since the last glacial. *Quaternary Science Reviews*, 122: 63–73.
- Li, J.Y., Dodson, J., Yan, H., Cheng, B., Zhang, X.J., Xu, Q.H., Ni, J., and Lu, F.Y., 2017. Quantitative precipitation estimates for the northeastern Qinghai-Tibetan Plateau over the last 18,000 years. *Journal of Geophysical Research: Atmospheres*, 122: 5132–5143.
- Li, Q., Wu, H.B., Yu, Y.Y., Sun, A.Z., Markovic, S.B., and Guo, Z.T., 2014. Reconstructed moisture evolution of the deserts in northern China since the Last Glacial Maximum and its implications for the East Asian Summer Monsoon. *Global and Planetary Change*, 121: 101–112.
- Liu, B., Jin, H.L., Sun, L.Y., Sun, Z., Niu, Q.H., Xie, S.B., and Li, G.H., 2014c. Holocene moisture change revealed by the Rb/Sr ratio of aeolian deposits in the southeastern Mu Us Desert, China. *Aeolian Research*, 13: 109–119.
- Liu, B., Jin, H.L., Sun, L.Y., Sun, Z., and Zhao, S., 2015. Geochemical evidence for Holocene millennial-scale climatic and environmental changes in the south-eastern Mu Us Desert, northern China. *International Journal of Earth Sciences*, 104: 1889–1900.
- Liu, B., Jin, H.L., Sun, Z., Miao, Y.F., Su, Z.Z., and Zhang, C., 2014b. Evidence of Holocene millennial-scale climatic change from Gonghe Basin peat deposit, northeastern Qinghai-Tibet Plateau. *Journal of Arid Environment*, 106: 1–10.
- Liu, B., Jin, H.L., Sun, L.Y., Sun, Z., Su, Z.Z., and Zhang, C.X., 2013a. Holocene climatic change revealed by aeolian deposits from the Gonghe Basin, northeastern Qinghai-Tibetan Plateau. *Quaternary International*, 296: 231–240.
- Liu, B., Jin, H.L., Sun, Z., Su, Z.Z., Zhao, S., and Zhang, C.X., 2013b. Extraction of sensitive grain-size component from the KE peat deposits of the Gonghe Basin and its implication for Holocene climatic and environmental change. *Marine Geology and Quaternary Geology*, 33(4): 125–134 (in Chinese with English Abstract).
- Liu, S.S., Huang, X.Z., Qiang, M.R., Lin, X.R., Bai, Z.J., and Peng, W., 2016. Vegetation and climate change during the Mid-Late Holocene reflected by the pollen record from Lake Genggahai, northeastern Tibetan Plateau. *Quaternary Science Reviews*, 36(2): 248–256 (in Chinese with English abstract).
- Liu, X.J., Colman, S.M., Brown, E.T., An, Z.S., Zhou, W.J., Jull, A.T.J., Huang, Y.S., Cheng, P., Liu, W.G., and Xu, H., 2014a. A climate threshold at the eastern edge of the Tibetan plateau. *Geophysical Research Letters*, 41(15): 5598–5604.
- Liu, X.J., Lai, Z.P., Yu, L.P., Sun, Y.J., and Madsen, D., 2012. Luminescence chronology of aeolian deposits from the Qinghai Lake area in the Northeastern Qinghai-Tibetan Plateau and its palaeoenvironmental implications. *Quaternary Geochronology*, 10: 37–43.
- Liu, X.Q., Dong, H.L., Rech, J.A., Matsumoto, R., Yang, B., and Wang, Y.B., 2008. Evolution of Chaka Salt Lake in NW China in response to climatic change during the latest Pleistocene-Holocene. *Quaternary Science Reviews*, 27: 867–879.
- Liu, X.Q., Shen, J., Wang, S.M., Wang, Y.B., and Liu, W.G.,

2007. Southwest monsoon changes indicated by oxygen isotope of ostracode shells from sediments in Qinghai Lake since the late Glacial. *Chinese Science Bulletin*, 52(4): 539–544.
- Liu, X.X., Sun, Y.B., Vandenberghe, J., Li, Y., and An, Z.S., 2018. Palaeoenvironmental implication of grain-size compositions of terrace deposits on the western Chinese Loess Plateau. *Aeolian Research*, 32: 202–209.
- Lu, H., Miao, X., Zhou, Y., Mason, J., Swinehart, J., Zhang, J., Zhou, L., and Yi, S., 2005. Late Quaternary aeolian activity in the Mu Us and Otindag dune fields (north China) and lagged response to insolation forcing. *Geophysical Research Letters*, 32: L21716.
- Lu, H., Yi, S., Liu, Z., Mason, J., Jiang, D., Cheng, J., Stevens, T., Xu, Z., Zhang, E., Jin, L., Zhang, Z., Guo, Z., Wang, Y., and Otto-Bliesner, B., 2013b. Variation of East Asian monsoon precipitation during the past 21 k.y. and potential CO<sub>2</sub> forcing. *Geology*, 41: 1023–1026.
- Lu, H., Yi, S., Xu, Z., Zhou, Y., Zeng, L., Zhu, F., Feng, H., Dong, L., Zhuo, H., Yu, K., Mason, J., Wang, X., Chen, Y., Lu, Q., Wu, B., Dong, Z., Qu, J., Wang, X., and Guo, Z., 2013a. Chinese deserts and sand fields in Last Glacial Maximum and Holocene Optimum. *Chinese Science Bulletin*, 58(23): 2775–2783.
- Lu, H., Zhao, C., Mason, J., Yi, S., Zhao, H., Zhou, Y., Ji, J., Swinehart, J., and Wang, C., 2011. Holocene climatic changes revealed by aeolian deposits from the Qinghai Lake area (northeastern Qinghai-Tibetan Plateau) and possible forcing mechanisms. *Holocene*, 21(2): 297–304.
- Lu, R.J., Jia, F.F., Gao, S.Y., Shang, Y., Li, J.F., and Zhao, C., 2015. Holocene aeolian activity and climatic change in Qinghai Lake basin, northeastern Qinghai-Tibetan Plateau. *Palaeogeography, Palaeoclimatology, Palaeoecology*, 430: 1–10.
- Mason, J., Lu, H., Zhou, Y., Miao, X., Swinehart, J.B., Liu, Z., Goble, R.J., and Yi, S., 2009. Dune mobility and aridity at the desert margin of northern China at a time of peak monsoon strength. *Geology*, 37(10): 947–950.
- Miao, Y.F., Jin, H.L., Liu, B., Herrmann, M., Sun, Z., and Wang, Y.P., 2015. Holocene climate change on the northeastern Tibetan Plateau inferred from mountain-slope pollen and non-pollen palynomorphs. *Review of Palaeobotany and Palynology*, 221:22–31.
- Murray, A.S., and Wintle, A.G., 2000. Luminescence dating of quartz using an improved single aliquot regenerative dose protocol. *Radiation Measurements*, 32: 57–73.
- Prescott, J.R., and Hutton, J.T., 1994. Cosmic ray contributions to dose rates for luminescence and ESR dating: large depths and long-term time variations. *Radiation Measurements*, 23, 497–500.
- Qiang, M.R., Chen, F.H., Song, L., Liu, X.X., Li, M.Z., and Wang Q., 2013b. Late Quaternary Aeolian activity in Gonghe Basin, northeastern Qinghai-Tibetan Plateau, China. *Quaternary Research*, 79: 403–412.
- Qiang, M.R., Chen, F.H., Wang, Z.T., Niu, G.M., and Song, L., 2010. Aeolian deposits at the southeastern margin of the Tengger Desert (China): Implications for surface wind strength in the Asian dust source area over the past 20,000 years. *Palaeogeography, Palaeoclimatology, Palaeoecology*, 286: 66–80.
- Qiang, M.R., Jin, Y.X., Liu, X.X., Song, L., Li, H., Li, F.S., and Chen, F.H., 2016. Late Pleistocene and Holocene aeolian sedimentation in Gonghe Basin, northeastern Qinghai-Tibetan Plateau: Variability, processes, and climatic implications. *Quaternary Science Reviews*, 132: 57–73.
- Qiang, M.R., Song, L., Chen, F.H., Li, M.Z., Liu, X.X., and Wang, Q., 2013a. A 16-ka lake-level record inferred from macrofossils in a sediment core from Genggahai Lake, northeastern Qinghai-Tibetan Plateau (China). *Journal of Paleolimnology*, 49: 575–590.
- Reimer, P.J., Bard, E., Bayliss, A., Beck, J.W., Blackwell, P.G., and Ramsey, C.B., 2013. IntCal13 and Marine13 radiocarbon age calibration curves 0–50,000 years cal BP. *Radiocarbon*, 55: 1869–1887.
- Shen, J., Liu, X.Q., Wang, S.M., and Ryo, M., 2005. Palaeoclimatic changes in the Qinghai Lake area during the last 18,000 years. *Quaternary International*, 136: 131–140.
- Stauch, G., Lai, Z.P., Lehmkuhl, F., and Schulte, P., 2018. Environmental changes during the late Pleistocene and the Holocene in the Gonghe Basin, north-eastern Tibetan Plateau. *Palaeogeography, Palaeoclimatology, Palaeoecology*, 509: 144–155.
- Stauch, 2016. Multi-decadal periods of enhanced aeolian activity on the northeastern Tibet Plateau during the last 2ka. *Quaternary Science Reviews*, 149: 91–101.
- Sun, J., Li, S., Han, P., and Chen, Y., 2006. Holocene environmental changes in the central Inner Mongolia, based on single-aliquot-quartz optical dating and multi-proxy study of dune sands. *Palaeogeography, Palaeoclimatology, Palaeoecology*, 233: 51–62.
- Sun, Y.G., Fang, H.B., Zhang, K., Zhao, F.Y., and Liu, S.Y., 2007. Step-like landform system of the Gonghe basin and the uplift of the Qinghai-Tibet Plateau and development of the Yellow River. *Geology in China*, 34(6): 1141–1147 (in Chinese with English abstract).
- Tian, S.H., Xiao G.Q., Dai, G.W., and Lai, Z.P., 2020. Recovery of early Holocene paleowind direction from the Gonghe Basin in northeastern Tibetan plateau and its implications for provenance of Chinese loess. *Quaternary Sciences*, 40(1): 95–104 (in Chinese with English Abstract).
- Uno, I., Eguchi, K., Yumimoto, K., Takemura, T., Shimizu, A., Uematsu, M., Liu, Z.Y., Wang, Z.F., Hara, Y., and Sugimoto, N., 2009. Asian dust transported one full circuit around the globe. *Nature Geoscience*, 2: 557–560.
- Wang, T., 2011. *Deserts and Aeolian Desertification in China*. Beijing: Science Press, 1–819.
- Wang, X. F., Zhao, H., Yang, H.Y., and Wang, K.Q., 2019. Optical dating reveals that the height of Earth's tallest megadunes in the Badain Jaran Desert of NW China is increasing. *Journal of Asian Earth Sciences*, 185: 104025.
- Wang, Y.J., Cheng, H., Edwards, R.L., He, Y.Q., Kong, Z.G., An, Z.S., Wu, J.Y., Kelley, M.J., Dykosko, C.A., and Li, Z.D., 2005. The Holocene Asian Monsoon: link to solar changes and North Atlantic Climate. *Science*, 308: 854–857.
- Wen, R.L., Xiao, J.L., Fan, J.W., Zhang, S.R., and Yamagata, H., 2017. Pollen evidence for a mid-Holocene East Asian summer monsoon maximum in northern China. *Quaternary Science Reviews*, 176: 29–35.
- Wu, D., Chen, F.H., Li, K., Xie, Y.W., Zhang, J.W., and Zhou, A.F., 2016. Effects of climate change and human activity on lake shrinkage in Gonghe Basin of northeastern Tibetan Plateau during the past 60 years. *Journal of Arid Land*, 8(4): 479–491.
- Xu, S.Y., Xu, D.F., and Shi, S.R., 1982. Aeolian sand deposits in the Gonghe basin, Qinghai province. *Journal of Desert Research*, 2 (3): 1–8 (in Chinese with English abstract).
- Xu, S.Y., Xu, D.F., and Shi, S.R., 1984. A discussion on the development of landforms and evolution of environments in the Gonghe Basin. *Journal of Lanzhou University*, 20, 146–157 (in Chinese with English abstract).
- Xu, Z.W., Mason, J.A., Lu, H.Y., Zhou, Y.L., Wu, J., and Han, Z.Y., 2017. Crescentic dune migration and stabilization: Implications for interpreting paleo-dune deposits as paleoenvironmental records. *Journal of Geographical Sciences*, 27 (11): 1341–1358.
- Xu, Z.W., Stevens, T., Yi, S.W., Mason, J.P., and Lu, H.Y., 2018. Seesaw pattern in dust accumulation on the Chinese Loess Plateau forced by late glacial shifts in the East Asian monsoon. *Geology*, 46(10): 871–874.
- Yang, B., Qin, C., Wang, J., He, M., Melvin, T.M., Osborn, T.J., and Briffa, K.R., 2014. A 3,500-year tree-ring record of annual precipitation on the northeastern Tibetan Plateau. *Proceedings of the national academy of sciences of the America*, 111: 2903–2908.
- Yang, L. M., and Zhu, B.Q., 2018. Environmental changes and landform evolution of the Alashan Plateau region during the Last Glacial period since 40 ka. *Acta Geological Sinica*, 92 (12): 2561–2581 (in Chinese with English Abstract).
- Yang, L.H., Zhou, J., Lai, Z.P., Long, H., and Zhang, J.R., 2010. Lateglacial and Holocene dune evolution in the Horqin

- dunefield of northeastern China based on luminescence dating. *Palaeogeography, Palaeoclimatology, Palaeoecology*, 296: 44–51.
- Yang, X., Liang, P., Zhang, D., Li, H., Rioual, P., Wang, X., Xu, B., Ma, Z., Liu, Q., Ren, X., Hu, F., He, Y., Rao, G., and Chen, N., 2019. Holocene aeolian stratigraphic sequences in the eastern portion of the desert belt (sand seas and sandy lands) in northern China and their palaeoenvironmental implications. *Science China Earth Sciences*, 62: 1302–1315.
- Yang, X., Scuderi, L., Paillou, P., Liu, Z., Li, H., and Ren, X., 2011. Quaternary environmental changes in the drylands of China—A critical review. *Quaternary Science Reviews*, 30: 3219–3233.
- Yang, X., Wang, X., Liu, Z., Li, H., Ren, X., Zhang, D., Ma, Z., Rioual, P., Jin, X., and Scuderi, L., 2013. Initiation and variation of the dune fields in semi-arid China—with a special reference to the Hunshandake Sandy Land, Inner Mongolia. *Quaternary Science Reviews*, 78: 369–380.
- Yu, L.P., and Lai, Z.P., 2014. Holocene climate change inferred from stratigraphy and OSL chronology of aeolian sediments in the Qaidam Basin, northeastern Qinghai–Tibetan Plateau. *Quaternary Research*, 81: 488–499.
- Zeng, L., Yi, S.W., Lu, H.Y., Chen, Y.Y., Lei, F., Xu, Z.W., Wang, X.Y., and Zhang, W.F., 2018. Response of dune mobility and pedogenesis to fluctuations in monsoon precipitation and human activity in the Hulunbuir dune field, northeastern China, since the last deglaciation. *Global and Planetary Change*, 168: 1–14.
- Zhang, J.W., Ma, X.Y., Qiang, M.R., Huang, X.Z., Li, S., Guo, X.Y., Henderson, A.C.G., Holmes, J.A., Chen, F.H., 2016. Developing inorganic carbon-based radioc and arbon chronologies for Holocene lake sediments in arid NW China. *Quaternary Science Reviews*, 144: 66–82.
- Zhang, W., Zhang, H., Ma, Y., Wang, X.Y., Mischke, S., and Zhang, C., 2019. Weak Summer Monsoon during the Early Holocene Inferred from the Dingxi Lujiagou Floodplain Lake–Eolian Sand Rhythm due to Solar Impacting. *Acta Geologica Sinica (English Edition)*, 93(3): 778–779.
- Zhang, X.Y., Gong, S.L., Zhao, T.L., Arimoto, R., Wang, Y.Q., and Zhou, Z.J., 2003. Sources of Asian dust and role of climate change versus desertification in Asian dust emission. *Geophysical Research Letters*, 30(24): 2272.
- Zhao, H., and Li, S.H., 2005. Internal dose rate to K-feldspar grains from radioactive elements other than potassium. *Radiation Measurements*, 40: 84–93.
- Zhao, H., Li, S.H., Li, B., and Li, G.Q., 2015. Holocene climate changes in westerly-dominated areas of central Asia: Evidence from optical dating of two loess sections in Tianshan Mountain, China. *Quaternary Geochronology*, 30: 188–193.

#### About the first author



LIU Bing, male, born in 1985 in Xinzhou City, Shanxi Province; doctor; graduated from Cold and Arid Regions Environmental and Engineering Research Institute, Chinese Academy of Sciences; Associate researcher of Northwest Institute of Eco-Environment and Resources, Chinese Academy of Science. He is now interested in the study on environment evolution and climate change in semi-arid and arid region. Email: liubing2014@lzb.ac.cn; Phone: 0931-4967495, 13519679543.

#### About the corresponding author



ZHAO Hui, male, born in 1973 in Pingliang City, Gansu Province; doctor; graduated from Department of Earth Sciences, The University of Hong Kong, Professor of Northwest Institute of Eco-Environment and Resources, Chinese Academy of Science. He is now interested in the study of the geochronology and the environment/climate changes in semi-arid and arid region. Email: hzhao@lzb.ac.cn; Phone: 0931-4967501, 13993145082.